Performance Studies of Pixel Hybrid Photon Detectors for the LHCb RICH Counters

G. Aglieri Rinella[1, 2], T. Gys[1], D. Piedigrossi[1], A. Van Lysebetten[1]

[1]CERN European Organization for Nuclear Research, CH1211 Geneva 23, Switzerland
[2]DIEPA Dept. Electrical Engineering, University of Palermo, V.le Delle Scienze, Palermo, Italy

Abstract: The Pixel Hybrid Photon Detector is a vacuum tube with a multi-alkali photo cathode, high voltage cross-focused electron optics and an anode consisting of a silicon pixel detector bump-bonded to a readout CMOS electronic chip fully encapsulated in the device. The Pixel HPD fulfils the requirements of the Ring Imaging Cherenkov counters of the LHCb experiment at LHC. The performances of the Pixel HPD will be discussed with reference to laboratory measurements, Cherenkov light imaging in recent beam tests, image distortions due to a magnetic field.

LHCb-PROC-2004-010
25/05/2004

1. Introduction

The LHCb experiment [1] requires positive kaon identification in the momentum range from 1 up to at least 100 GeV/c. This is provided by a set of Ring Imaging Cherenkov detectors [2] with 3 different radiators, aerogel, C_4F_{10} and CF_4, with refractive indexes of 1.03, 1.0014 and 1.0005. A balance between the aberrations from the optical system, Rayleigh scattering, light losses and position resolution sets the requirements for the photon detectors. In particular good single photon detection capabilities with excellent spatial resolution on a large active area are to be provided. These stringent requirements are fully satisfied by the novel Pixel Hybrid Photon Detectors (HPD) developed for LHCb [3].

The HPD (fig 1.1) is a vacuum tube of 80 mm diameter, 115 mm height. Its entrance window is made by quartz and a S20 blue enhanced multi-alkali photo cathode is deposited on its inner surface. Peak Quantum Efficiency (QE) up to 27% at 240 nm wavelength was measured. Photo electrons emitted from the cathode are accelerated in a 20 kV cross-focusing electron optics with a demagnification factor around 5. The anode assembly is fully encapsulated in the vacuum envelope. The anode is constituted by a pixel silicon detector bump bonded onto a CMOS readout chip. The 300 μm thick reverse biased p-n silicon detector is divided into 32×256 pixels of 500×62.5 μm^2. Each pixel is bump bonded to one of the 8192 read-out channels of LHCBPIX1. Every channel has front-end analogue circuitry with 25 ns peaking time and 40 MHz digital section with coincidence logic and memories following an adjustable threshold discriminator. The photoelectrons release about 5000 e-h pairs in the detector. A typical threshold value of the electronics is 1300 e with a spread of 134 e. The signals are digitally ORed to form a matrix of 32×32 pixels corresponding to sensitive areas of 2.5×2.5 mm^2 on the entrance window of the tube. The HPDs in the LHCb experiment are closed packed and give an active coverage of 70% of the total detector area of 2.8 m^2. The digital readout is done via 32 binary lines fed through the anode carrier.

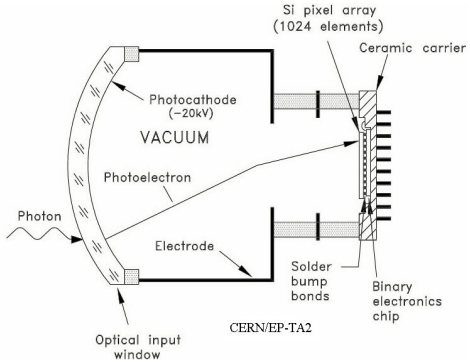

Fig. 1.1: A schematic picture of a Pixel HPD

2. Performance studies

The performances of the HPD prototypes have been evaluated in a laboratory set-up, using a fast pulsed LED light source [4].

Typical high voltage scans results are shown in fig. 2.1 for different values of the discriminating thresholds. The probability to record a hit when a photo electron reaches the anode is less than 1 due to three main reasons: the channel's threshold distribution, a probability that an electron doesn't release all its energy being back-scattered from the silicon detector and the charge sharing between adjacent pixels. A measurement of the detection efficiency has been realized. To this goal the pulse-height spectrum of the detector signal has been determined; it is shown in fig. 2.2 where single electron peaks are clearly separated. The HPD's detection efficiency is 88% at 20 kV.

There are two intrinsic main sources of background in an HPD. Dark-counts, due to the thermo-ionic emission from the cathode, give a hit rate of the order of 1 KHz/cm^2 on the anode surface at room temperature. A photoelectron can ionise a residual gas molecule in the tube, the ion being then accelerated to the cathode where it releases electrons, which then travel to the anode. This signal is correlated, delayed of 250 ns, to an original hit and it's typically constituted of large pixel clusters because many photoelectrons are released from the ion hitting the cathode. The probability of this ion-feedback has been measured as 0.5% per original photoelectron.

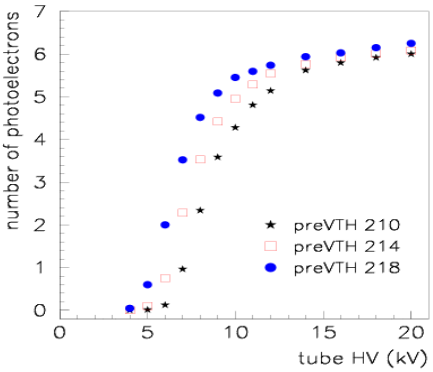

Fig 2.1: High Voltage scans for different discriminating thresholds.

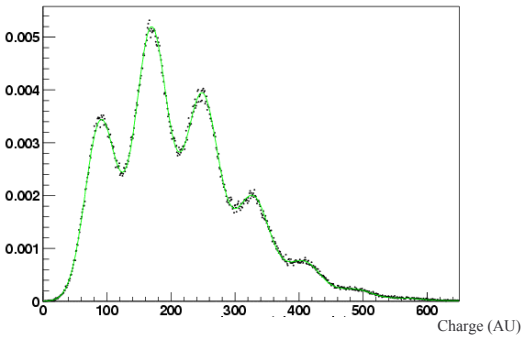

Fig 2.2: The pulse height spectrum of the silicon detector current.

3. *Beam test measurements*

First prototypes of 40 MHz HPDs were tested in two beam tests at CERN in August and October 2003. The Cherenkov radiators were air, N_2 and Aerogel. The analysis of events, including a fit to the photon hits on the HPD, allowed the determination of the Cherenkov angles and of the resolution in the test set-up. Measured Cherenkov angles for 10 Gev/c pions and electrons in N_2 were respectively: 20.6±1.3 mrad and 25.6±1.5 mrad, in accordance to the expected resolution of the HPDs. High voltage and detector bias voltage scans are in agreement with the results from the laboratory.

A measurement of the HPD detection efficiency has been done using the test beam data. The radiator refractive index curve, losses for reflections at optical interfaces, HPD cathode Q.E. curves are used for calculating the expected average photon yield according to the classic formula:

$$N = \int_{\lambda} \frac{2\pi Z^2 \alpha L}{\lambda^2}\left[1 - \frac{1}{n^2(\lambda)\beta^2}\right] \cdot R_M(\lambda) \cdot T(\lambda) \cdot QE(\lambda) d\lambda.$$

The result is to be compared with the measured average cluster number, after correcting for multiple hits probability. Results for two HPD prototypes are shown in table 3.1 and are in agreement with the determination done using the pulsed light source.

Table 3.1
Beam test measurement of Detection Efficiency

HPD	N	Measured Average of p.e.	Detection Efficiency
#8	11.6 (±0.7)	10.1	87.1 ±5.3
#9	12.8 (±0.8)	10.6	82.8 ±5.2

4. *Magnetic distortions*

The HPDs will operate in the fringe field of the LHCb dipole magnet. An external magnetic field will influence the trajectory of the photoelectrons causing the distortion of the cathode image and will reduce the space resolution of the HPD. Iron shielding boxes will enclose the photon detector planes both in RICH 1 and in RICH 2 to protect the devices from the magnet. The residual magnetic flux density inside the shielding structure is specified to be less than 2.5 mT in RICH 1 and less than 1.0 mT in the RICH 2. The position of the photon detectors is such that the magnetic field will have a dominant component parallel to the axes of the HPDs in RICH 1, while it will be mainly orthogonal to the tubes in RICH 2.

There is the need for a local individual magnetic shielding of each HPD. The local shield reduces the magnetic flux in the tube and the image distortions to a level that allows their offline compensation, restoring the space resolution. In our set-up a cylindrical shield of MuMetal, a high magnetic permeability alloy, surrounded the tube. The local

shield has an internal diameter of 86 mm, 0.9 mm thickness, 140 mm length and it protrudes of 25 mm from the HPD entrance window. Proper electrical insulation from the tube electrodes had to be provided.

The experimental set-up is constituted by an HPD tube, a dedicated ASIC based, PC controlled read-out system, a DC LED source supported by a double axis motorized positioning system. Helmholtz coils are used to apply a magnetic flux to the set-up. Photons are shined on the HPD window positioning the LED at various points in a double-cross pattern. The measurements quantify the distortions of the pattern recorded when a known magnetic field is applied. Data have been taken with and without the local magnetic shield installed, varying the magnetic flux density values and changing the angle between the **B** field and the axis of the HPD, which is also the axis of symmetry of the electron optics **E** field. Results with applied **B** field forming angles of 0° ($\mathbf{B}_{\parallel}$) and 90° ($\mathbf{B}_{\perp}$) with the tube axis are presented.

The distortion expected and observed when an axial field $\mathbf{B}_{\parallel}$ is applied is a non-uniform rotation of the image due to the spiralling of the electrons around the field direction, while they are accelerating from the cathode to the anode. Fig. 4.1a shows the effect. Also a dilatation of the image in the radial direction is observed. The demagnification law is the function, which relates the radial coordinate of the light spot at the HPD entrance window plane to the radial coordinate of focused electrons at anode plane. Fig. 4.2 shows the demagnification laws with no field applied and with a 1.5 mT axial field on a bare HPD. A 5.0 mT field applied to a shielded HPD causes distortions of roughly the same entity than a 1.5 mT applied without the shield. A non-linear curve is expected even in the absence of magnetic field, because the electron optics design optimised active area coverage. Data points are well fitted with second order polynomials (table 4.1). The rotation of the image around the tube axis with an axial field applied is a function of the radial coordinate as data of tables 4.2 and 4.3 show. The effect of local shielding is roughly equivalent to a factor 3-6 reduction of the field. The most sensitive region of the tube is the one in proximity of the cathode. The residual field is higher in proximity of the axis causing a larger rotation of the pattern close to the centre.

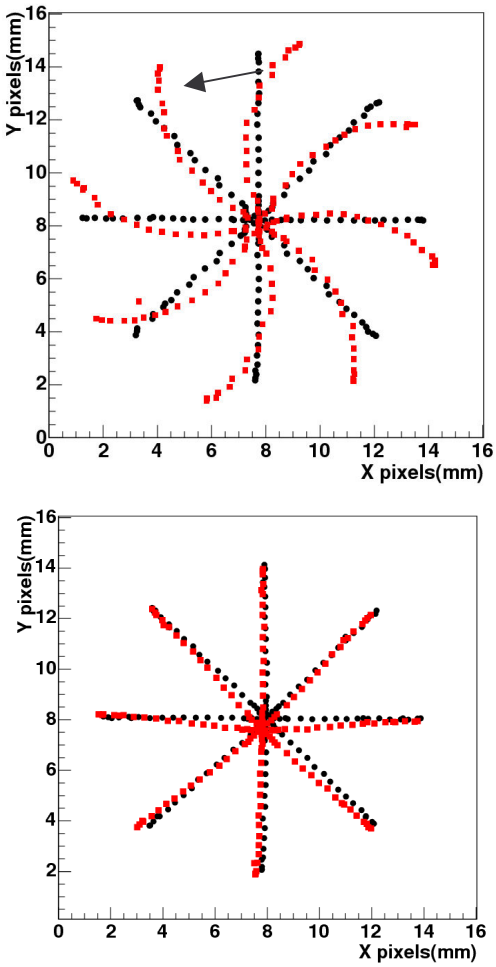

Fig 4.1 a, b: Double cross pattern distortions on a shielded HPD with an axial (a) 5.0 mT field applied and a transverse (b) 5.0 mT field applied. The distorted patterns are plotted with squares, overlapped to the reference (0 mT) image.

The effect of a transverse $\mathbf{B}_{\perp}$ field is a non-uniform translation of the image in a direction normal to the magnetic field (fig 4.1b). The entity of displacements is smaller than in the axial case. A stronger shielding effect for a transverse field is evident. Largest displacements are measured in proximity of the pattern centre. Effects observed in a shielded tube in a 5.0 mT field are similar to those observed with a bare HPD in a field of less than 0.25 mT. Data reported in tables 4.4 and 4.5 show a maximum displacement of half pixel (0.5 mm) with a 3.0 mT field applied on a shielded tube.

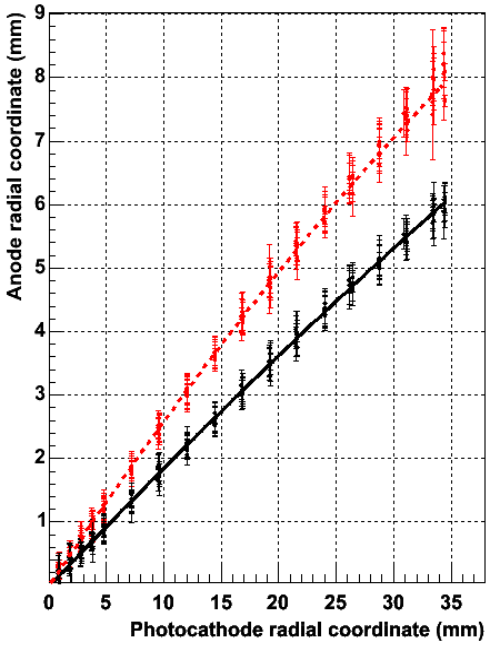

Fig 4.2: Unshielded HPD demagnification law. Continuous line: fit to 0 mT data. Dashed: fit to data with $\mathbf{B}_{\parallel}$ 1.5 mT field.

Table 4.1
Coefficients of polynomial fits of fig. 4.2.

$B_{\parallel}$ [mT]	1st order coefficient	2nd order coefficient
0	0.190 ± 0.004	-0.0004 ± 0.0001
1.5	0.272 ± 0.004	-0.0012 ± 0.0002

5. *Conclusions*

The measurements realized on the HPDs in a magnetic field with the magnetic shielding show that the devices would properly operate in the fringe field of the LHCb experiment magnet. In particular no coverage loss was observed even in magnetic flux densities as high as 5.0 mT. The effects of a transverse field $\mathbf{B}_{\perp}$ are less significant than those of an axial $\mathbf{B}_{\parallel}$ field. The distortions observed have been accurately quantified and a parameterisation is feasible and ongoing. This will serve as a basis for the definition of an off-line compensation procedure of the acquired data. It is also foreseen the development of a RICH photon detectors overall calibration procedure based on the projection of a pre-defined optimal light pattern before and after switching on the LHCb experiment dipole magnet.

Table 4.2
Rotation of pattern points as a function of axial magnetic flux density in an unshielded HPD at two different distances from electron optics axis.

$B_{\parallel}$ [mT]	Δφ (r=16 mm) [rad]	Δφ (r=35 mm) [rad]
0.25	0.25	0.25
0.5	0.45	0.4
0.75	0.6	0.55
1.0	0.75	0.7
1.5	1	0.7

Table 4.3
Rotation of pattern points as a function of axial magnetic flux density in a shielded HPD at two different distances from electron optics axis.

$B_{\parallel}$ [mT]	Δφ (r=16 mm) [rad]	Δφ (r=35 mm) [rad]
3.0	0.55	0.3
4.0	0.7	0.45
5.0	0.85	0.65

Tables 4.4 (left), 4.5 (right)
Maximum displacements of pattern points at various transverse magnetic flux densities values in an unshielded (4.4) and shielded (4.5) HPD.

$B_{\perp}$ [mT]	Max displ. Δd [mm]
0.25	0.9
0.5	1.56
0.75	2.15
1.0	2.76
1.5	3.53

$B_{\perp}$ [mT]	Max displ. Δd [mm]
3.0	0.262
4.0	0.373
5.0	0.517

Acknowledgements
Authors wish to thank M. Moritz, T. Bellunato, O. Ullaland, R. Forty and C.D'Ambrosio.

References

[1] The LHCb Collaboration, *LHCb Technical Proposal*, CERN/LHCC/1998-004 February 1998.
[2] The LHCb Collaboration, *LHCb RICH TDR*, CERN/LHCC/2000-0037, 7 September 2000.
[3] T. Gys, *The pixel hybrid photon detectors for the LHCb-RICH project*, Nucl. Instr. And Meth. A465 (2001) 240.
[4] M. Moritz et al., *Performance Study of New Pixel Hybrid Photon Detector Prototypes for the LHCb RICH counter,* IEEE Transactions on Nuclear Science, June 2004